

Accurate dust temperature determination in a $z = 7.13$ galaxy

Tom J. L. C. Bakx^{1,2*}, Laura Sommovigo³, Stefano Carniani³, Andrea Ferrara³,
Hollis B. Akins⁴, Seiji Fujimoto^{5,6}, Masato Hagimoto¹, Kirsten K. Knudsen⁷,
Andrea Pallottini³, Yoichi Tamura¹ and Darach Watson^{5,6}

¹ *Division of Particle and Astrophysical Science, Graduate School of Science, Nagoya University, Aichi 464-8602, Japan.*

² *National Astronomical Observatory of Japan, 2-21-1, Osawa, Mitaka, Tokyo 181-8588, Japan.*

³ *Scuola Normale Superiore, Piazza dei Cavalieri 7, 56126, Pisa, Italy*

⁴ *Department of Physics, Grinnell College, 1116 Eighth Ave., Grinnell, IA 50112, USA*

⁵ *Cosmic Dawn Center (DAWN), Copenhagen, Denmark*

⁶ *Niels Bohr Institute, University of Copenhagen, Jagtvej 128, Copenhagen, Denmark*

⁷ *Department of Earth and Space Sciences, Chalmers University of Technology, Onsala Space Observatory, SE-43992 Onsala, Sweden*

Accepted 2021 September 3. Received 2021 September 3; in original form 2021 August 10.

ABSTRACT

We report ALMA Band 9 continuum observations of the normal, dusty star-forming galaxy A1689-zD1 at $z = 7.13$, resulting in a $\sim 4.6\sigma$ detection at 702 GHz. For the first time these observations probe the far infrared (FIR) spectrum shortward of the emission peak of a galaxy in the Epoch of Reionization (EoR). Together with ancillary data from earlier works, we derive the dust temperature, T_d , and mass, M_d , of A1689-zD1 using both traditional modified blackbody spectral energy density fitting, and a new method that relies only on the [C II] 158 μm line and underlying continuum data. The two methods give $T_d = (42_{-7}^{+13}, 40_{-7}^{+13})$ K, and $M_d = (1.7_{-0.7}^{+1.3}, 2.0_{-1.0}^{+1.8}) \times 10^7 M_\odot$. Band 9 observations improve the accuracy of the dust temperature (mass) estimate by $\sim 50\%$ (6 times). The derived temperatures confirm the reported increasing T_d -redshift trend between $z = 0$ and 8; the dust mass is consistent with a supernova origin. Although A1689-zD1 is a *normal* UV-selected galaxy, our results, implying that $\sim 85\%$ of its star formation rate is obscured, underline the non-negligible effects of dust in EoR galaxies.

Key words: galaxies: high-redshift — galaxies: evolution — galaxies: formation — galaxies: individual (A1689-zD1) — ISM: dust, extinction — submillimetre: galaxies

1 INTRODUCTION

Atacama Large Millimeter/submillimeter Array (ALMA) observations have revealed the presence of dust in galaxies approaching the epoch of reionization (EoR; e.g., Capak et al. 2015; Willott et al. 2015; Barisic et al. 2017; Laporte et al. 2017). This was somewhat surprising, since UV studies mapping out the cosmic star-formation rate density (SFRD) to $z \sim 10$ suggested a dearth of dust at the high-redshift end based on the blue UV slopes of low-stellar mass high- z galaxies (β_{UV} ; e.g., Finkelstein et al. 2015; Bouwens et al. 2016). Initially, the strong FIR emission at $z > 7$ revealed by ALMA observations was attributed to the presence of unexpectedly large dust masses (M_d) in the observed high- z galaxies, which was hard to reconcile with known dust production mechanisms that operate on that timescale (predominantly SN and

grain growth; see Leńniewska & Michałowski 2019 and references therein for the latest constraints).

This resulted in the so-called *dust budget crisis*, which also impacted star-formation history (SFH) estimates of high-redshift galaxies (e.g., Mawatari et al. 2020; Roberts-Borsani et al. 2020). The stringent constraints on SNe dust production, coupled with the large deduced dust masses at $z > 7$, required very early stellar populations originating at $z \sim 14$ (Tamura et al. 2019). However, the conclusions on the dust masses were heavily dependent on the assumed (cold) dust temperatures ($T_d \sim 30 - 40$ K) for these high- z sources, since in most cases only a single data point was available in the FIR continuum. Recent observations (e.g., Bakx et al. 2020) and theoretical studies (e.g. Behrens et al. 2018; Sommovigo et al. 2020) have suggested the presence of warm dust in several high- z galaxies ($T_d > 60$ K), alleviating the large dust mass requirements set by their observed L_{FIR} ($M_d \propto T_d^{-(4+\beta_d)}$ at fixed L_{FIR} , where typically $1.0 < \beta_d < 3.0$).

* E-mail: bakx@a.phys.nagoya-u.ac.jp (Nagoya University)

Unfortunately, the large uncertainties on derived T_d at high- z still hinder accurate SFH studies.

Partially due to the lack of knowledge on the dust temperature at high- z , the total fraction of obscured star-formation beyond $z > 4$ is also largely unknown (Novak et al. 2017; Casey et al. 2018; Bouwens et al. 2020; Gruppioni et al. 2020; Schouws et al. 2021; Talia et al. 2021; Zavala et al. 2021). This has strong implications for the cosmic SFRD; for example, some of these recent works suggest that there is no steep drop-off in SFRD at $z > 3$ (e.g., Gruppioni et al. 2020), which could indicate that we might be underestimating the contribution of highly obscured systems to the SFRD at $z > 3$ due to the bias towards UV bright objects. On top of that, most studies calculate the obscured star-formation rates and far-infrared luminosities of single sources either by assuming a dust temperature, and/or by scaling directly from the infrared excess (IRX = $L_{\text{FIR}}/L_{\text{UV}}$)- β_{UV} relation. Both approaches suffer from the inherent uncertainty in dust temperature (since obscured SFR and IRX both scale with $T^{4+\beta_d}$).

Moreover, the validity of IRX- β_{UV} relation at high- z demands that the UV and dust-emitting regions to be co-spatial, relying on the absorbed UV emission to be re-emitted at far-infrared wavelengths. However, observations suggest the possibility of spatial separation between these regions in several sources at $z = 4-6$ (e.g., Faisst et al. 2017) and at $z \sim 7-8$ sources (e.g., Carniani et al. 2017a; Laporte et al. 2019 and Tamura et al. in prep.). In fact, this *spatial separation* scenario between UV and IR is also supported by theoretical studies and simulations (Behrens et al. 2018; Cochrane et al. 2019; Liang et al. 2019; Sommovigo et al. 2020). A deviating IRX- β_{UV} relation would impact the results of galaxies at high- z (Le Fèvre et al. 2020; Fudamoto et al. 2020), and will impact re-emission studies (e.g., MAGPHYS; da Cunha et al. 2008 and CIGALE; Boquien et al. 2019) which will be prevalent in the ALMA + JWST era.

In this letter, we use the band 9 observations to estimate the dust properties of a $z = 7.1$ galaxy from the spectrum directly in order to measure the obscured star-formation directly. We describe the source and data in Section 2, the fitting techniques in Section 3 and the implications in Section 4.¹

2 TARGET AND OBSERVATIONS

A1689-zD1 was identified in Bradley et al. (2008) as a bright ($m_{\text{AB}} \sim 25$) $z > 7$ galaxy. Due to the foreground galaxy cluster (A1689; Struble & Rood 1999), it is magnified² by $\mu \simeq 9.3$ (Knudsen et al. 2017). Its intrinsic UV magnitude indicates it is a sub- L^* galaxy representing the bulk of galaxies at $z = 7$ (Ono et al. 2018). Band 6 observations at 1.3 mm by Watson et al. (2015) reported the first detection of dust beyond redshift 7, and indicated an intrinsic star-formation rate of $\sim 12 M_{\odot} \text{yr}^{-1}$. Notably, the estimated dust mass of

¹ Throughout this paper, we assume a flat Λ -CDM cosmology with the best-fit parameters derived from the *Planck* results (Planck Collaboration et al. 2016), which are $\Omega_m = 0.307$, $\Omega_{\Lambda} = 0.693$ and $h = 0.678$.

² While μ is high, there is only little shear, and we do not account for any differential lensing effects in this paper

Table 1. Continuum and fitting properties of A1689-zD1

	λ [mm]	$F_{\nu}^{\text{int}} [\mu\text{Jy}]^{\dagger}$	Reference
Band 9	0.427	154 ± 37	This work
Band 8	0.728	180 ± 39	Inoue et al. (2020)
Band 7	0.873	143 ± 15	Knudsen et al. (2017)
Band 6	1.33	60 ± 11	Watson et al. (2015)
	SED fit	[C II]-based	SED fit (no B9)
T_d [K]	42^{+13}_{-7}	40^{+13}_{-7}	38^{+35}_{-13}
β_d	$1.61^{+0.60}_{-0.75}$	2.03^{\ddagger}	$1.78^{+0.55}_{-0.97}$
M_d [$10^7 M_{\odot}$] [†]	$1.7^{+1.3}_{-0.7}$	$2.0^{+1.8}_{-1.0}$	$2.4^{+11}_{-1.9}$
L_{FIR} [$10^{11} L_{\odot}$] [†]	$1.9^{+0.5}_{-0.4}$	$2.2^{+4.1}_{-1.0}$	$1.5^{+3.0}_{-0.6}$
\log_{10} IRX	$1.0^{+0.1}_{-0.1}$	$1.0^{+0.5}_{-0.3}$	$0.8^{+0.5}_{-0.2}$
M_d/SN [M_{\odot}] [†]	$0.4^{+0.3}_{-0.1}$	$0.6^{+0.6}_{-0.3}$	$0.8^{+3.0}_{-0.7}$

Notes: [†] Corrected for the magnification assuming $\mu = 9.3$ from Knudsen et al. (2017). [‡] β_d is fixed to 2.03.

this *normal* galaxy (assuming 35 K) was found in tension to star-formation history and dust production estimates in Leńniewska & Michałowski (2019).

In this letter, we combine the existing data on A1689-zD1 reported in Watson et al. (2015), Knudsen et al. (2017) and Inoue et al. (2020) with archival band 9 data from (Program ID: 2019.1.01778.S, P.I. D. Watson), see Table 1. We use the [C II] luminosity as reported in Knudsen et al. in prep., which is $(6.1 \pm 0.7) \times 10^8 L_{\odot}$, and use their value for spectroscopic redshift, $z_{\text{spec}} = 7.13$.

For the band 9 (Baryshev et al. 2015) data, the source was observed for 95 min. in baselines ranging from 14 to 312 m. The lower and upper sidebands covered the contiguous frequency ranges of 690.4 to 697.6 and of 706.5 to 713.6 GHz. We assume a typical flux accuracy of 10%. The continuum image is produced with CASA pipeline version 5.6.1-8 (McMullin et al. 2007), using natural weighting, a taper of 0.5 arcseconds, and excluding any channels within 1000 km/s of the [O III] 52 μm emission at 711.4 GHz. Figure 1 shows the resulting image with a 0.61 by 0.67 arcsecond beam with a beam position angle of 75 degrees, with an r.m.s. level of $210 \mu\text{Jy beam}^{-1}$. Using CASA’s IMFIT routine, we spatially integrate the emission using a 2D Gaussian profile. This results in a flux of 1.43 ± 0.31 mJy ($\sim 4.6\sigma$; excluding calibration flux), with an apparent (or lensed) beam-deconvolved size of 0.81 ± 0.26 by 0.38 ± 0.22 arcsec at a position angle of 44 ± 38 degrees. The emission appears co-spatial to the UV-emission seen in Knudsen et al. (2017), although we leave further discussion of this to Knudsen et al. in prep.

3 METHODS

3.1 Spectral fitting

Figure 2 shows the modified black-body (eq. 8 in Sommovigo et al. 2021) fitted to the continuum points reported in Table 1. We use equations 12 and 18 from da Cunha et al. (2013) to account for the heating of dust by and decreasing contrast against the CMB, respectively. We approximate the dust mass absorption coefficient (κ_{ν}) as $\kappa_{\star} (\nu/\nu_{\star})^{\beta_d}$,

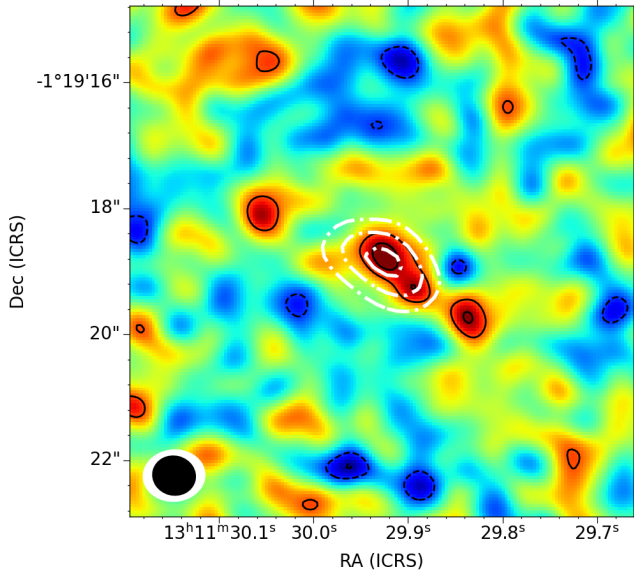


Figure 1. The tapered band 9 data (*background and black contours*; drawn at -3 , -2 , 2 and 3σ) is shown against the band 8 continuum emission (*white contours*; drawn at 5 , 7 and 10σ). The continuum emissions appears co-spatial, and we find a 4.6σ dust detection in band 9.

with (κ_*, ν_*) as $(10.41 \text{ cm}^2/\text{g}, 1900 \text{ GHz})$ from [Draine \(2003\)](#). We use the `emcee` MCMC-fitting routine, and allow M_d , T_d and β_d to vary freely using flat priors, resulting in a magnification-corrected dust mass of $1.7^{+1.3}_{-0.7} \times 10^7 M_\odot$, a dust temperature of 42^{+13}_{-7} K and a β_d of $1.61^{+0.60}_{-0.75}$. We note that the spectrum appears well-represented by a single modified black-body. For comparison, we also fit the spectral energy distribution (SED) without band 9 data, with an upper limit on β_d of 2.5 to ensure convergence, and find significantly larger errors across the board. If we take a fiducial $\beta_d = 1.8$ (e.g., [Casey 2012](#); [Faisst et al. 2020](#)), we find a more accurate dust temperature of 39^{+4}_{-5} K , however there is no improvement on the error of dust mass ($2.0^{+1.4}_{-0.7} \times 10^7 M_\odot$) nor luminosity ($1.7^{+0.5}_{-0.4} \times 10^{11} L_\odot$). The accuracy of these later parameters thus depends solely on observational uncertainties, indicating that we fully trace the dust emission in this source.

3.2 Dust temperature from [C II] emission

We use the novel method proposed in [Sommovigo et al. \(2021\)](#) to derive the dust temperature in galaxies, based on the combination of 1900 GHz continuum and the overlying [C II] line emission. We provide a brief summary of this method below; for further details and verification of this method on 19 local galaxies, three galaxies at $z \gtrsim 4$, and a $z \sim 6.7$ simulated galaxy, we refer to [Sommovigo et al. \(2021\)](#).

We relate the observed [C II] luminosity to the total dust mass via the gas mass and a gas-to-dust ratio (assumed to scale linearly with the metallicity, which is justified down to $Z \lesssim 0.1 Z_\odot$, see [James et al. 2002](#); [Draine & Li 2007](#); [Galliano et al. 2008](#); [Leroy et al. 2011](#)). The gas mass and [C II] luminosity are related through a conversion factor $M_{\text{gas}} = \alpha_{\text{CII}} L_{\text{CII}}$. This conversion factor α_{CII} is analytically derived from the

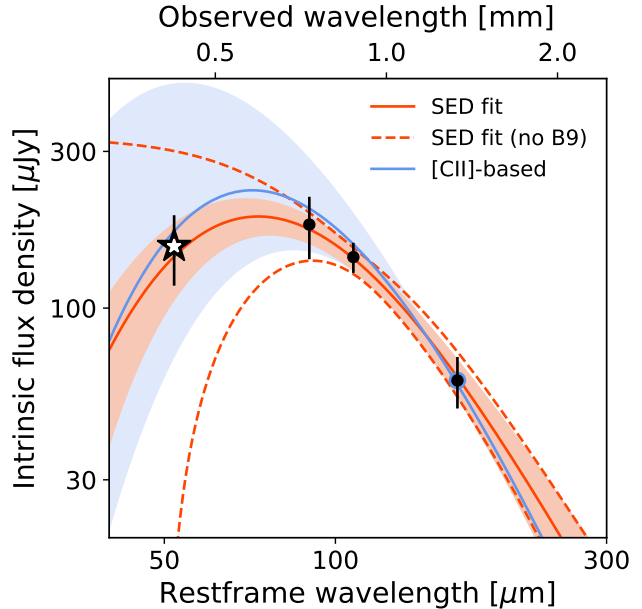


Figure 2. We fit a modified black-body (*red line and fill*) to the observed data points of A1689-zD1, including the band 9 data point (*star*). The [C II]-based spectrum (*blue line and fill*) is fit solely to the $158 \mu\text{m}$ continuum data point (*blue*), and it predicts a consistent galaxy spectrum, providing confidence in the [C II]-based method for this specific source even at $50 \mu\text{m}$ rest-frame. For comparison, the *dashed red lines* show the spread in SEDs fitted without band 9 data, which results in a twice larger error in dust temperature, and a sixfold increase in the error in dust mass.

combination of the de Looze relation ([De Looze et al. 2014](#)) and the Kennicutt–Schmidt relation ([Kennicutt 1998](#), hereafter, KS). Two parameters are added in the expression for α_{CII} in order to account for both (i) the expected offset from the KS-relation (i.e., the burstiness of the SF of a galaxy parametrized by κ_s) and (ii) the observed larger extension of [C II] with respect to stellar emission at high- z (up to 1.5–3 times larger; [Carniani et al. 2017b, 2018, 2020](#); [Matthee et al. 2017, 2019](#); [Fujimoto et al. 2019, 2020, 2021](#); [Ginolfi et al. 2020](#); [Herrera-Camus et al. 2021](#)).

We fit a modified blackbody to derive the dust temperature using the neighbouring continuum emission at $\sim 1900 \text{ GHz}$ rest-frame wavelength, assuming a fixed $\beta_d = 2.03$, which is based on the [Draine \(2003\)](#) predictions for the Milky Way and the Small Magellanic Cloud. Within this fitting routine, both the burstiness parameter (κ_s) and the metallicity are largely uncertain. In order to constrain the dust temperature, two broad physical constraints are placed: (i) The dust mass cannot exceed the maximal dust mass producible by supernovae (SNe), assuming all the SNe metal yield ($\sim 2 M_\odot$ per SN) ends up locked into dust grains; (ii) The dust-obscured star formation³ ([Kennicutt 1998](#); [Madau & Dickinson 2014](#)), cannot significantly (by 1 order of magnitude) exceed the SFR deduced from [C II] using the relation from [De Looze et al. \(2014\)](#) for starbursts. Apply-

³ This IR luminosity-to-SFR conversion factor, $1.73 \times 10^{-10} M_\odot \text{ yr}^{-1} / L_\odot$, is valid for a Salpeter 1 – 100 M_\odot IMF, which we assume consistently throughout the paper

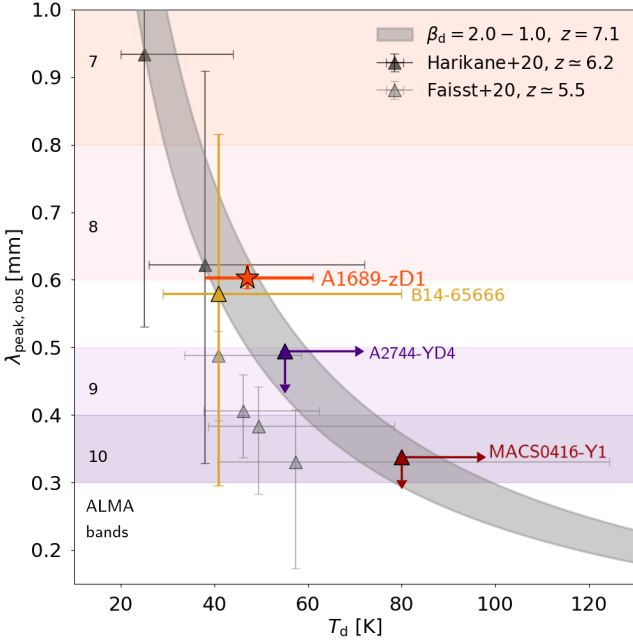


Figure 3. Observed peak wavelength $\lambda_{\text{peak,obs}}$ is shown against dust temperature T_d for a given dust emissivity index, β_d . The grey shaded region shows $\lambda_{\text{peak,obs}}(T_d)$ at redshift $z = 7.1$ for $\beta_d = 2.0 - 1.0$. We show the sources with reported dust temperatures beyond $z > 5$ (Faisst et al. 2020; Harikane et al. 2020; Sugahara et al. 2021; Bakx et al. 2020; Laporte et al. 2019). The shaded regions show the wavelength ranges probed by ALMA bands 7 – 10. Without band 9, we cannot probe the FIR peak on both sides and accurately estimate T_d through SED fitting, while for lower-redshift observations band 10 might even be required to accurately trace the SED.

ing our method to A1689-zD1, we find a dust temperature $T_d = 40^{+13}_{-7}$ K and mass of $M_d = 2.0^{+1.8}_{-1.0} \times 10^7 M_\odot$. These values are obtained assuming a wide range of values for the metallicity $Z = 0.2 - 1 Z_\odot$, and the burstiness parameter $\kappa_s = 1 - 50$ (Vallini et al. 2021). For our further discussion of dust production mechanisms, we note that the removal of the dust production constraint does not influence the derived quantities.

4 IMPLICATIONS

The dust temperature and mass estimates from the [C II]-based method agree with the results from the direct SED fitting, which adds confidence to the method from Sommovigo et al. (2021). As shown in Table 1, band 9 observations reduce the uncertainty in the dust temperature by $\sim 50\%$, which translates to much-improved estimate on the far-infrared luminosity and dust mass estimate. In Figure 3, we show the observed peak emission wavelength ($\lambda_{\text{peak,obs}}$) of galaxies at $z > 5$ against our current best-estimates for T_d and β_d . To guide the eye, we include the trend of $\lambda_{\text{peak,obs}}$ with T_d for $\beta_d = 1 - 2$ at $z = 7.1$. We also overlay the wavelengths of the ALMA bands 7 through 10. We calculate this $\lambda_{\text{peak,obs}}$ using

$$\frac{\lambda_{\text{peak,obs}}}{\text{mm}} = \frac{14.42 (1+z) (T_d/\text{K})^{-1}}{W(-a e^{-a}) + a},$$

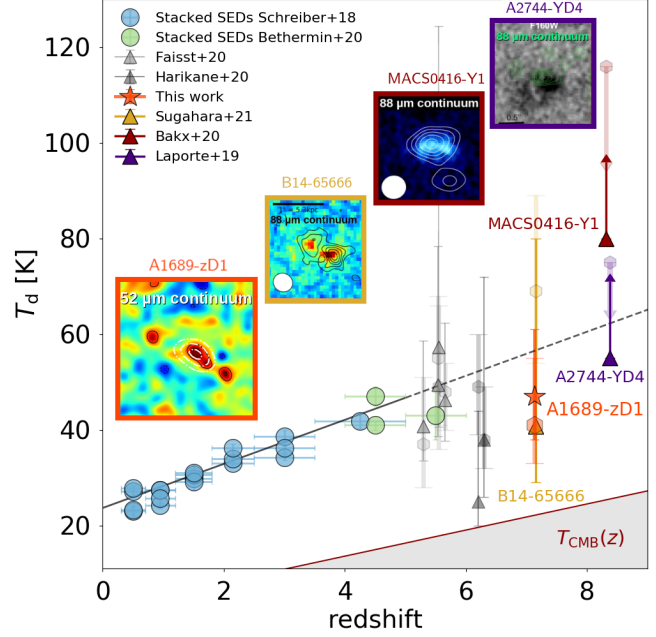


Figure 4. Dust temperature T_d in “normal” (main-sequence) galaxies as a function of redshift. The newest T_d estimates for A1689-zD1 are shown in red (*star* for SED-fit and *hexagon* for the [C II]-based result). Dust temperatures obtained from stacked SEDs (blue and green circles) increase linearly with redshift up to $z = 6$. We highlight all the continuum detected sources at $z > 7$ with small post-stamps, and include their estimated T_d based on both SED fits (*triangles*) and the [C II]-based method (*hexagons*; Faisst et al. 2020; Harikane et al. 2020; Sugahara et al. 2021; Bakx et al. 2020; Laporte et al. 2019). The addition of band 9 data significantly reduces the uncertainty on the dust temperature of this source with respect to the other high- z sources, which are not observed in that band.

where $a = 3 + \beta_d$ and W is the Lambert W function. This is the wavelength at which the continuum spectrum F_ν peaks in frequency units (e.g., Figure 2). This is an important distinction to keep in mind when visualising $\lambda_{\text{obs,peak}}$ from the analogy to Wien’s law, which provides the peak of the spectrum when reported in wavelength units F_λ .

Particularly for galaxies at lower redshifts and at higher temperatures, short-wavelength observations are crucial to estimate the dust temperature, whereas band 8 might be able to probe the emission peak for cold $z > 8$ galaxies. In the foreseeable future, the high bands of ALMA (9 and 10) are the only instrument capable of probing this regime, until such missions as the Origins Space Telescope⁴ (Meixner et al. 2019).

Accurate estimates of the the dust-obscured fraction of the star-formation rate require strong constraints on the dust temperature, as $\text{SFR}_{\text{obs}} \propto L_{\text{FIR}} \propto M_d T_d^{4+\beta_d}$. Our band 9 observations confirm that this relatively-cold ($T_d \sim 40 - 60$ K) system has a very large obscured fraction of the SFR around $\sim 85\%$ ($\text{SFR}_{\text{obs}} = 33 \pm 9 M_\odot \text{yr}^{-1}$, whereas⁵ $\text{SFR}_{\text{UV}} = 5.7 \pm 0.3 M_\odot \text{yr}^{-1}$), even though it was selected to be

⁴ <https://asd.gsfc.nasa.gov/firs/docs/>

⁵ derived using the magnification-corrected $L_{\text{UV}}/10^{10} L_\odot = 2.28 \pm 0.1$ (Hashimoto et al. 2019), and the UV luminosity-to-unobscured SFR conversion factor in Madau & Dickinson (2014).

UV-bright. The dust-obscured ratio is higher than the 61% found for the typically more-massive ALPINE survey (Le Fèvre et al. 2020; Faisst et al. 2020; Fudamoto et al. 2020; Béthermin et al. 2020; Khusanova et al. 2021) at $z = 5.5$, although this 61% is expected to decrease with higher redshift. Albeit extreme, our dust-obscured ratio is in line with recent results (both theoretical and observational) suggesting that we might have been underestimating the dust-obscured contribution to the total SFR in $z > 4$ galaxies (see e.g. Novak et al. 2017; Gruppioni et al. 2020). On the other hand, some studies of similarly-massive, UV-bright sources at very high- z ($z \sim 7$; e.g., Bouwens et al. 2021; Schouws et al. 2021) have so far failed to detect dust continuum at $158 \mu\text{m}$ in half of their sources, even though their average stellar mass is similar to those of A1689-zD1. These undetected sources might have low dust contents, but that does not guarantee low obscured star-formation fractions, since it is possible that this dust is warm and is mainly emitting at wavelengths shorter than the currently observed ones (mainly $158 \mu\text{m}$ rest-frame). In fact, while the continuum around $158 \mu\text{m}$ of MACS0416_Y1 (Tamura et al. 2019; Bakx et al. 2020) has yet to be seen, its spectrum is indicative of a similar obscured fraction to A1689-zD1 (i.e., 94 to 85% for $\beta_d = 1.5$ to 2), even though Y1’s UV-observed stellar mass is one order of magnitude lower than A1689-zD1.

The selection towards UV-bright sources might also bias towards lower fractions of obscured-to-total star-formation rate. With the discovery of so-called optically-dark galaxies (e.g., Simpson et al. 2014; Franco et al. 2018; Hatsukade et al. 2018; Wang et al. 2019; Yamaguchi et al. 2019; Williams et al. 2019; Algera et al. 2020; Romano et al. 2020; Talia et al. 2021; Toba et al. 2020; Umehata et al. 2020; Zhou et al. 2020; Shibuya et al. 2021; Smail et al. 2021), we know of the existence of galaxies without detections in optical wavelengths at high redshift. These sources, by definition, have exceedingly high obscured fractions and might well account for a substantial fraction of the SFRD at high redshift (Alcalde Pampliega et al. 2019; Gruppioni et al. 2020; Zavala et al. 2021). The typical obscured star-formation rate fraction across all $z > 7$ galaxies might thus be higher than predicted by UV-selected samples alone, with for example Gruppioni et al. (2020) predicting an increase in SFRD of 17% at $z = 5$ by this population.

Recently, attempts to quantify dust obscuration at high- z have used a linear scaling between dust temperature (and L_{IR} given a fixed β_d) and redshift (see e.g. Schreiber et al. 2018; Bouwens et al. 2020; Vijayan et al. 2021). Other recent works have suggested that this linearly increasing $T_d - z$ trend flattens at $z > 4$ (Liang et al. 2019; Faisst et al. 2020). In Figure 4 we show the reported linear evolution of the dust temperature with redshift, adding our latest results for A1689-zD1, and where available, include the results from the method in Sommovigo et al. (2021). The observed dust temperature for A1689-zD1 is compatible with both a flattening (Liang et al. 2019; Faisst et al. 2020) and a linear (Schreiber et al. 2018) $T_d - z$ evolution. Meanwhile, the exceedingly-large scatter in T_d at the highest redshifts (particularly at $z > 7$) prevents us from reaching a definitive conclusion on this observed evolution. Much of this scatter is due to observational limitations, and only through further short-wavelength observations of galaxies beyond $z > 7$ can we distinguish the possible scenarios. Part of the scatter

could also be due to a larger source-to-source variation in T_d , which is for example seen by the large diversity of galaxies among the typically more-massive ALPINE sources (Le Fèvre et al. 2020). Such source-to-source variation can only be identified by larger unbiased samples looking at the dust-obscured star-formation at high redshift. Here we note that an increased intrinsic scatter in dust temperature would significantly boost the resulting dust-obscured star-formation rate, given their strong dependence of star-formation rate on dust temperature, similar to an Eddington-type bias.

Due to the large obscured fraction of the SFR in A1689-zD1, one might naively expect that this galaxy also contains an exceedingly large dust mass. Instead, the dust mass derived from SED fitting implies a dust yield of $y_d = 0.4^{+0.3}_{-0.1} M_\odot$ per SN. This estimate is almost an order of magnitude more accurate than the one derived without band 9 data, and most importantly, it is consistent with latest SN dust production constraints by Leńniewska & Michałowski (2019) based on the expected number of SNe given its stellar mass estimate. They find at most a $y_d = 1.1 M_\odot$ per SN, derived in the extreme case of no dust destruction/ejection. We note that SN yield is still highly debated, with other works suggesting that dust destruction processes might only spare $0.1 M_\odot$ per SN (e.g., Matsuura et al. 2015, 2019; Slavin et al. 2020). In this extreme case, inter-stellar medium grain growth (Mancini et al. 2015; Michałowski 2015) or more exotic dust production mechanisms might well be required at $z > 7$, such as dust produced in supershells (e.g., Martínez-González et al. 2021) or in the wake of Wolf-Rayet stars (e.g., Lau et al. 2021).

REFERENCES

- Alcalde Pampliega B., et al., 2019, *ApJ*, **876**, 135
 Algera H. S. B., et al., 2020, *ApJ*, **903**, 139
 Bakx T. J. L. C., et al., 2020, *MNRAS*, **493**, 4294
 Barisic I., et al., 2017, *ApJ*, **845**, 41
 Baryshev A. M., et al., 2015, *A&A*, **577**, A129
 Behrens C., Pallottini A., Ferrara A., Gallerani S., Vallini L., 2018, *MNRAS*, **477**, 552
 Béthermin M., et al., 2020, *A&A*, **643**, A2
 Boquien M., Burgarella D., Roehlly Y., Buat V., Ciesla L., Corre D., Inoue A. K., Salas H., 2019, *A&A*, **622**, A103
 Bouwens R. J., et al., 2016, *ApJ*, **833**, 72
 Bouwens R., et al., 2020, *ApJ*, **902**, 112
 Bouwens R. J., et al., 2021, arXiv e-prints, p. arXiv:2106.13719
 Bradley L. D., et al., 2008, *ApJ*, **678**, 647
 Capak P. L., et al., 2015, *Nature*, **522**, 455
 Carniani S., et al., 2017a, *A&A*, **605**, A42
 Carniani S., et al., 2017b, *A&A*, **605**, A42
 Carniani S., et al., 2018, *MNRAS*, **478**, 1170
 Carniani S., et al., 2020, *MNRAS*, **499**, 5136
 Casey C. M., 2012, *MNRAS*, **425**, 3094
 Casey C. M., et al., 2018, *ApJ*, **862**, 77
 Cochrane R. K., et al., 2019, *MNRAS*, **488**, 1779
 De Looze I., et al., 2014, *A&A*, **568**, A62
 Draine B., 2003, *Annual Review of Astronomy and Astrophysics*, **41**, 241
 Draine B. T., Li A., 2007, *ApJ*, **657**, 810
 Faisst A. L., et al., 2017, *ApJ*, **847**, 21

- Faisst A. L., Fudamoto Y., Oesch P. A., Scoville N., Riechers D. A., Pavesi R., Capak P., 2020, *MNRAS*, **498**, 4192
- Finkelstein S. L., et al., 2015, *ApJ*, **810**, 71
- Franco M., et al., 2018, *A&A*, **620**, A152
- Fudamoto Y., et al., 2020, *A&A*, **643**, A4
- Fujimoto S., et al., 2019, *ApJ*, **887**, 107
- Fujimoto S., et al., 2020, *ApJ*, **900**, 1
- Fujimoto S., et al., 2021, *ApJ*, **911**, 99
- Galliano F., Dwek E., Chianal P., 2008, *ApJ*, **672**, 214
- Ginolfi M., et al., 2020, *A&A*, **633**, A90
- Gruppioni C., et al., 2020, *A&A*, **643**, A8
- Harikane Y., et al., 2020, *ApJ*, **896**, 93
- Hashimoto T., et al., 2019, *Pub. Astron. Soc. Japan*, p. 70
- Hatsukade B., et al., 2018, *Pub. Astron. Soc. Japan*, **70**, 105
- Herrera-Camus R., et al., 2021, *A&A*, **649**, A31
- Inoue A. K., Hashimoto T., Chihara H., Koike C., 2020, *MNRAS*, **495**, 1577
- James A., Dunne L., Eales S., Edmunds M. G., 2002, *MNRAS*, **335**, 753
- Kennicutt Robert C. J., 1998, *ApJ*, **498**, 541
- Khusanova Y., et al., 2021, *A&A*, **649**, A152
- Knudsen K. K., Watson D., Frayer D., Christensen L., Gallazzi A., Michałowski M. J., Richard J., Zavala J., 2017, *MNRAS*, **466**, 138
- Laporte N., et al., 2017, *ApJL*, **837**, L21
- Laporte N., et al., 2019, *MNRAS*, **487**, L81
- Lau R. M., et al., 2021, *ApJ*, **909**, 113
- Le Fèvre O., et al., 2020, *A&A*, **643**, A1
- Leroy A. K., et al., 2011, *The Astrophysical Journal*, **737**, 12
- Leńniewska A., Michałowski M. J., 2019, *A&A*, **624**, L13
- Liang L., et al., 2019, *MNRAS*, **489**, 1397
- Madau P., Dickinson M., 2014, *ARA&A*, **52**, 415
- Mancini M., Schneider R., Graziani L., Valiante R., Dayal P., Maio U., Ciardi B., Hunt L. K., 2015, *MNRAS*, **451**, L70
- Martínez-González S., Silich S., Tenorio-Tagle G., 2021, *MNRAS*, **507**, 1175
- Matsuura M., et al., 2015, *ApJ*, **800**, 50
- Matsuura M., et al., 2019, *MNRAS*, **482**, 1715
- Matthee J., et al., 2017, *The Astrophysical Journal*, **851**, 145
- Matthee J., et al., 2019, *The Astrophysical Journal*, **881**, 124
- Mawatari K., et al., 2020, *ApJ*, **889**, 137
- McMullin J. P., Waters B., Schiebel D., Young W., Golap K., 2007, in *Astronomical Data Analysis Software and Systems XVI*. p. 127
- Meixner M., et al., 2019, arXiv e-prints, p. [arXiv:1912.06213](https://arxiv.org/abs/1912.06213)
- Michałowski M. J., 2015, *A&A*, **577**, A80
- Novak M., et al., 2017, *A&A*, **602**, A5
- Ono Y., et al., 2018, *Pub. Astron. Soc. Japan*, **70**, S10
- Planck Collaboration et al., 2016, *A&A*, **594**, A13
- Roberts-Borsani G. W., Ellis R. S., Laporte N., 2020, *MNRAS*, **497**, 3440
- Romano M., et al., 2020, *MNRAS*, **496**, 875
- Schouws S., et al., 2021, arXiv e-prints, p. [arXiv:2105.12133](https://arxiv.org/abs/2105.12133)
- Schreiber C., Elbaz D., Pannella M., Ciesla L., Wang T., Franco M., 2018, *A&A*, **609**, A30
- Shibuya T., Miura N., Iwadate K., Fujimoto S., Harikane Y., Toba Y., Umayahara T., Ito Y., 2021, arXiv e-prints, p. [arXiv:2106.03728](https://arxiv.org/abs/2106.03728)
- Simpson J. M., et al., 2014, *ApJ*, **788**, 125
- Slavin J. D., Dwek E., Mac Low M.-M., Hill A. S., 2020, *ApJ*, **902**, 135
- Smail I., et al., 2021, *MNRAS*, **502**, 3426
- Sommovigo L., Ferrara A., Pallottini A., Carniani S., Gallerani S., Decataldo D., 2020, *MNRAS*, **497**, 956
- Sommovigo L., Ferrara A., Carniani S., Zanella A., Pallottini A., Gallerani S., Vallini L., 2021, *MNRAS*, **503**, 4878
- Struble M. F., Rood H. J., 1999, *ApJS*, **125**, 35
- Sugahara Y., et al., 2021, arXiv e-prints, p. [arXiv:2104.02201](https://arxiv.org/abs/2104.02201)
- Talia M., Cimatti A., Giuliatti M., Zamorani G., Bethermin M., Faisst A., Le Fèvre O., Smolčić V., 2021, *ApJ*, **909**, 23
- Tamura Y., et al., 2019, *ApJ*, **874**, 27
- Toba Y., et al., 2020, *ApJ*, **899**, 35
- Umehata H., et al., 2020, *A&A*, **640**, L8
- Vallini L., Ferrara A., Pallottini A., Carniani S., Gallerani S., 2021, *MNRAS*, **505**, 5543
- Vijayan A. P., et al., 2021, arXiv e-prints, p. [arXiv:2108.00830](https://arxiv.org/abs/2108.00830)
- Wang T., et al., 2019, *Nature*, **572**, 211
- Watson D., Christensen L., Knudsen K. K., Richard J., Gallazzi A., Michałowski M. J., 2015, *Nature*, **519**, 327
- Williams C. C., et al., 2019, *ApJ*, **884**, 154
- Willott C. J., Carilli C. L., Wagg J., Wang R., 2015, *ApJ*, **807**, 180
- Yamaguchi Y., et al., 2019, *ApJ*, **878**, 73
- Zavala J. A., et al., 2021, *ApJ*, **909**, 165
- Zhou L., et al., 2020, *A&A*, **642**, A155
- da Cunha E., Charlot S., Elbaz D., 2008, *MNRAS*, **388**, 1595
- da Cunha E., et al., 2013, *ApJ*, **766**, 13

DATA AVAILABILITY

The data underlying this article will be shared on reasonable request to the corresponding author.

ACKNOWLEDGEMENTS

We would like to thank the anonymous referee for their insightful comments and suggested additions. This paper makes use of the following ALMA data: ADS/JAO.ALMA 2011.1.00319.S, 2012.1.00216.S, 2013.1.01064.S, 2016.1.00954.S, and 2019.1.01778.S. TB and YT acknowledge funding from NAOJ ALMA Scientific Research Grant Numbers 2018-09B and JSPS KAKENHI No. 17H06130. LS, SC, AF, AP acknowledge support from the ERC Advanced Grant INTERSTELLAR H2020/740120 (PI: Ferrara). The Cosmic Dawn Center is funded by the Danish National Research Foundation under grant No. 140. This project has received funding from the European Union's Horizon 2020 research and innovation program under the Marie Skłodowska-Curie grant agreement No. 847523 'INTERACTIONS'. DW and SF are supported by Independent Research Fund Denmark grant DFF-7014-00017 Any dissemination of results must

indicate that it reflects only the author's view and that the Commission is not responsible for any use that may be made of the information it contains.